1-30-2024

Superconductivity of Amorphous and Crystalline Re–Lu Films

Serafim Teknowijoyo
Chapman University

Armen Gulian
Chapman University, gulian@chapman.edu

Recommended Citation

Serafim Teknowijoyo and Armen Gulian 2024 *Supercond. Sci. Technol.* 37 035005 https://doi.org/10.1088/1361-6668/ad1f7e

Superconductivity of Amorphous and Crystalline Re–Lu Films

Superconductivity of amorphous and crystalline Re–Lu films

OPEN ACCESS
IOP Publishing
Superconductor Science and Technology
Supercond. Sci. Technol. **37** (2024) 035005 (9pp)
https://doi.org/10.1088/1361-6668/ad1f7e

Superconductivity of amorphous and crystalline Re–Lu films

Serafim Teknowijoyo and Armen Gulian*

Advanced Physics Laboratory, Institute for Quantum Studies, Chapman University, Burtonsville, MD 20866, United States of America

E-mail: gulian@chapman.edu

Received 24 September 2023, revised 20 December 2023
Accepted for publication 17 January 2024
Published 30 January 2024

Abstract

We report on superconducting properties of a novel material: rhenium-lutetium films. Different compositions of Re_xLu binary are explored from $x \approx 3.8$ to close to pure Re stoichiometry. The highest critical temperature, up to $T_c \approx 7$ K, is obtained for $x \approx 10.5$ in accordance with electron dispersive spectroscopy results. Depending on the deposition conditions, polycrystalline or amorphous films are obtainable, both of which are interesting for practical use. Crystalline structure of polycrystalline phase is identified as a non-centrosymmetric superconductor using grazing incidence x-ray diffractometry. Superconducting properties were characterized both resistively and magnetically. Magnetoresistivity and AC/DC susceptibility measurements allowed us to determine H_{c1} and H_{c2} of these films, as well as estimate coherence length $\xi(0)$ and magnetic penetration depth $\lambda_L(0)$. We also provide information on surface morphology of these films. Demonstration of superconductivity in this material justifies the point of view that Lu plays a role of group 3 transition metal in period 6 of the Periodic table of elements. Then, in analogy with Re–Nb, Re–Ti, Re–Hf and Re–Zr, one can expect that crystalline Re–Lu also breaks time-reversal symmetry. If that is proven by future experiments, in combination with noncentrosymmetric feature, these films could be used for forming nonreciprocal current devices, such as superconducting diodes, without involvement of external magnetic fields.

Keywords: superconducting films, crystal structure, magnetoresistance, critical temperature, lattice parameters, superconducting diodes

1. Introduction

Non-centrosymmetric superconductors (NCS) with broken time-reversal symmetry (TRS) are related to 'hot topics' in contemporary research of quantum materials. Theory predicts that a nonreciprocal response (such as directional transport and propagation of electrons, photons, phonons, magnons) in quantum materials with broken inversion symmetry can occur ubiquitously when the TRS is further broken [1]. Breaking the TRS is possible in presence of magnetic field. This field may be of intrinsic nature, for example, because of magnetochiral effect or spin-orbital interaction [2, 3], or be applied externally. The inversion symmetry is broken in NCS; in case of ordinary superconductors, the methods of nanopatterning can be used. This suggestion was experimentally verified; as a result, many experimental designs have been reported with nonreciprocal current control, such as diodes, transistors, quadristors, etc, see articles [4–12] to name a few. However, in all of these works, the TRS was broken by a magnetic field of external origin. One recent report [13] avoids magnetic field and achieved superconducting diode effect (SDE) via chiral eutectic superconductor Sr_2RuO_4 in $Nb/Ru/Sr_2RuO_4$ topological Josephson junction. Application of these type of

* Author to whom any correspondence should be addressed.

materials inherently breaking TRS is a promising way to abandon the necessity of external magnetic fields in designing SDE-based devices. To succeed with this line of development, it is attractive to employ materials with possibly higher critical temperature and available easily in a thin film form. From that point of view, it is reasonable to explore Re-based compounds, such as Re–Nb [14], Re–Ti [15, 16], Re–Hf [17] and Re–Zr [18]. Pure rhenium is centrosymmetric. However, the compounds named belong to NCS. Moreover, muon spectroscopy revealed broken time-reversal symmetry [14–18], complementing their NCS origin. Thin-film superconductors of these materials can be easily deposited, and they are resistant to oxidation, have low resistivity, and/or are compatible with high magnetic fields [19, 20]. As such, SDE and other similar effects in these liquid-helium temperature superconductors look promising in quantum computation technologies [21–23].

Rhenium itself belongs to transition metals, and in bulk form at ambient conditions, it superconducts below $T_c \approx 1.7$ K [24–26]. In a thin film form T_c is higher [24, 27–30] and can reach values up to 6 K. Compounds of Re with other transition metals allowed material scientists to achieve not only higher values of T_c, but also, as was mentioned above, to demonstrate broken TRS in addition to NCS. The physical mechanisms yielding broken TRS in these materials are not yet clear. As shown in 1985 by Volovik and Gor'kov, magnetic superconductors may exist in non-trivial superconducting classes both with singlet and triplet pairing [31]. From this point of view it is interesting to explore the occurrence of superconductivity in Re–Lu compositions, since there is an arguable opinion that the lanthanide Lu is closer to transition metals than La itself [32]. In particular, the Periodic table group IIIB representatives Sc and Y are non-superconductive at ambient conditions, and so is Lu, while La has $T_c = 4.9$ K. Low-lying nonhydrogenic f-orbitals are absent in Y, Sc and Lu but present in La. Structure of metals, their oxides and chlorides are similar for Y, Sc and Lu, but different for La. More details on these and other features and relevant references can be found in reference [33]. Thus, Lu can be considered as an interesting representative of transition metals' group. However, Re–Lu superconductor has not yet been reported either in bulk or thin film form.

To partially close this gap, we report here on superconducting properties of amorphous and polycrystalline Re–Lu films with critical temperature of complete transition up to about 7 K[1]. We studied morphology of the films, magnetotransport and magnetic susceptibility which allowed us to estimate basic features of superconducting state, such as the critical fields, coherence length, and London penetration depth.

[1] This value is higher than that of other Re-based compounds except ReNb.

2. Experimental details

The Re–Lu films were prepared via magnetron sputtering in our ATC series UHV Hybrid deposition system (AJA International, Inc.) with a base pressure of 1×10^{-8} Torr. The Re target (ACI Alloys, Inc. 99.99% purity) was accommodated inside of a 1.5" DC gun. The Lu target (Heeger Materials, Inc. purity Lu/TREM 99.99%) was placed inside of a 2" DC gun. The sapphire substrate (AdValue Technology, thickness 650 μm, C-cut) was cleaned thoroughly with isopropyl alcohol before it was mounted on the holder. In our chamber's configuration, the substrate holder is at the center of the chamber facing upwards, while the (five) sputtering guns are located at the top. The substrate is rotated in plane throughout the whole deposition process to ensure a homogeneous deposition layer over the whole surface. Our predeposition *in-situ* cleaning of the substrate typically involves heating it up to 900 °C for 10 min followed by a gentle bombardment of Ar^+ at 600 °C for 5–10 min using a Kaufman ion source at 45° to the substrate surface. Then the temperature was raised back to 900 °C and kept at that value for 30 min. Afterwards, the temperature was reduced to 600 °C and simultaneous deposition took place for 10 min, at pressure 3–4 mTorr (the increase to 4 mTorr was sometimes required for plasma stability; such action did not change the stoichiometry and just non-essentially reduced the deposition speed), with gun power 250–260 W and anode voltage 460-605 V for Re, and with gun power 45-90 W and anode voltage correspondingly 275-325 V for Lu. Keeping the Re gun power constant, and varying the sputtering power of Lu from case to case allowed us to vary the values of x in composition Re_xLu (see table 1). After the deposition, the temperature was again raised to 900 °C for *in-situ* annealing for 30 min and then cooled down to ambient temperature. All the heating/cooling protocols consistently used a 30 °C min^{-1} ramp rate.

The deposition rate at these regimes was about 10 nm min^{-1} which was obtained *ex-situ* using x-ray reflectivity method (via Rigaku SmartLab diffractometer). These measurements can also be used to characterize the quality of the films which turned out to be rather high (see appendix C). Resistive superconducting transitions of samples and their magnetoresistive properties were characterized using PPMS-DynaCool (Quantum Design). Simultaneous multichannel measurements were used to analyze the homogeneity of various thickness films (appendix B). The vibrational sample magnetometer as well as AC/DC susceptometer options of PPMS were exploited for magnetic characterization of films. Lastly, the stoichiometry was also checked by the scanning electron microscope (SEM) Hitachi SU3500 equipped with the electron dispersive x-ray spectroscopy (EDS) Oxford Instruments X-MAX-20^N. The details are presented in appendix A.

Table 1. Re/Lu stoichiometry ratios from EDS, with T_c and deposition parameters.

Re/Lu	P_{Lu}, W	T_{substr}, °C	Pressure, mTorr	T_c, K	Crystallinity
3.8	90	600	3	5.25	Amorphous
7.4	55	30	4	6.1	Amorphous
7.5	70	600	3	5.8	Amorphous
10.5	55	600	3	6.95	Polycrystalline
11.5	55	600	3	6.75	Polycrystalline
>99	45	600	4	6.3	Polycrystalline

Grazing incidence diffraction (GID) data were taken using Rigaku SmartLab x-ray diffractometer to determine whether the films are amorphous or polycrystalline. Details of the analysis of our GID data, including the evidence of small inclusions of pure Re existent in the material are presented in Results. For these reasons, the compositional characterization of films by the value of x should be understood throughout the whole article as an approximate value introduced for the convenience of description. It corresponds to the EDS outcome at a given energy (20 keV) and characterizes the film's material as a whole, but not the precise formula of the Re–Lu superconducting phase.

3. Results

Our initial choice of x for examining Re_xLu composition was $x \sim 4$, in rough analogy with the well-known NCS superconductor $Re_{0.82}Nb_{0.18}$, known for its breaking of TRS. The composition with $x \sim 3.8$ indeed turned out to be an amorphous superconductor with $T_c \approx 5.3$ K, see figure 1(a). Figure 1(b) demonstrates that for $x \sim 10.5$, both field cooled (FC) and zero field cooled (ZFC) curves of magnetic moment measurement show magnetic flux expulsion consistent with the behavior of type-II superconductors. We will discuss this in greater detail below.

Lowering the relative concentration of the co-deposited Lu first increased and then decreased the T_c, with the optimum $T_c \approx 7$ K corresponding to $x \sim 10 - 11$ (shown also in figure 1). Though the normal state resistivities of these two compositions are not much different, they have very different surface morphologies, figure 2.

Comparative characteristics of our films with various values of x are shown in table 1. To characterize the crystalline structure of our films we used grazing incidence x-ray diffractometry which minimizes the reflections of the substrate, figure 3. In this way it was recognized that the films with $x \sim 3.8$ are amorphous, and those with $x \sim 10$ are polycrystalline. While GID is distinct from the powder diffraction method, it is still meaningful to compare our polycrystalline spectrum with the powder diffraction database. Using the online Crystallography Open Database, we matched our spectrum with the powder data of $Re_{24}Zr_5$ (figure 3), which allowed us to draw qualitative justification that the films belong to the $I\bar{4}3m$ space group within the 217 cubic crystal symmetry. However, the observed peak at 43° suggests that the film also

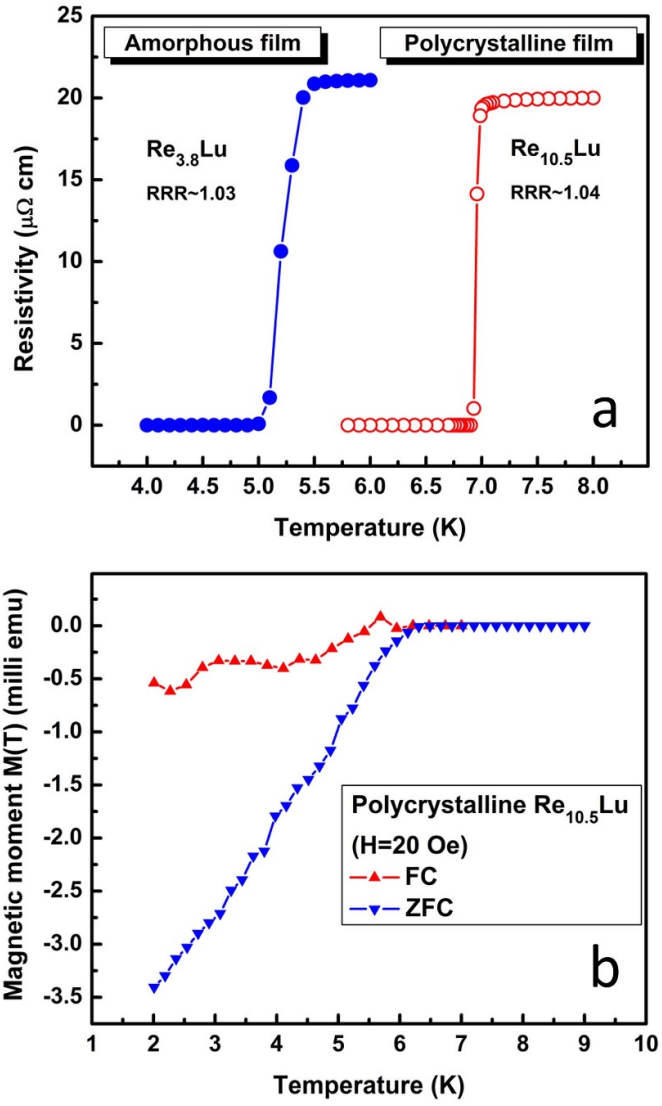

Figure 1. (a) Resistive superconducting transition in amorphous (at $x = 3.8$) and polycrystalline (at $x = 10.5$) Re_xLu films; (b) Magnetic flux expulsion below T_c by polycrystalline $Re_{10.5}Lu$ film. The FC curve shows weaker diamagnetic response indicating the presence of trapped fluxes, consistent with type-II superconductor behavior.

contains pure Re phase. Hence, taking both the GID and EDS results into account, the superconducting phase of the film is likely to have stoichiometry $5 \lesssim x \lesssim 10.5$. A proper phase identification to find the precise atomic percentage of compositional elements requires a powder x-ray diffraction performed

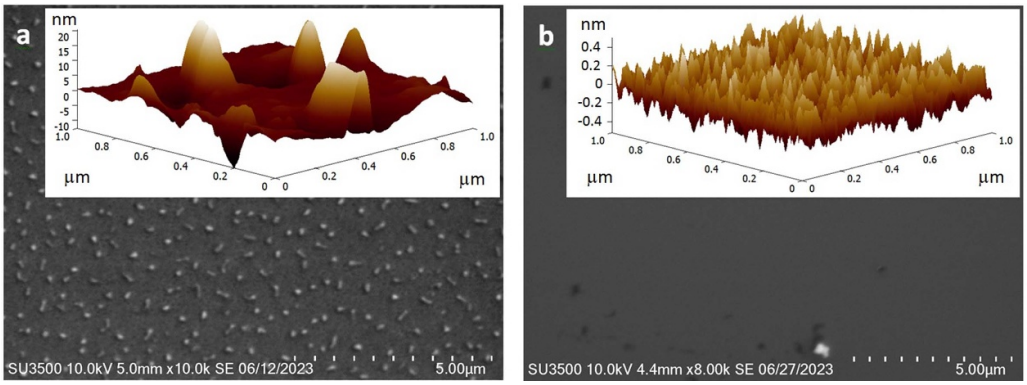

Figure 2. Surface morphology of Re_xLu films obtained by scanning electron microscope (in these SEM images, the intergraticule distance is 0.5 μm) in case of amorphous (panel (a), $x = 3.8$) and crystalline (panel (b), $x = 10.5$) films. Insets show 3D image of corresponding film's surface obtained via atomic force microscope (NT-MDT NTEGRA).

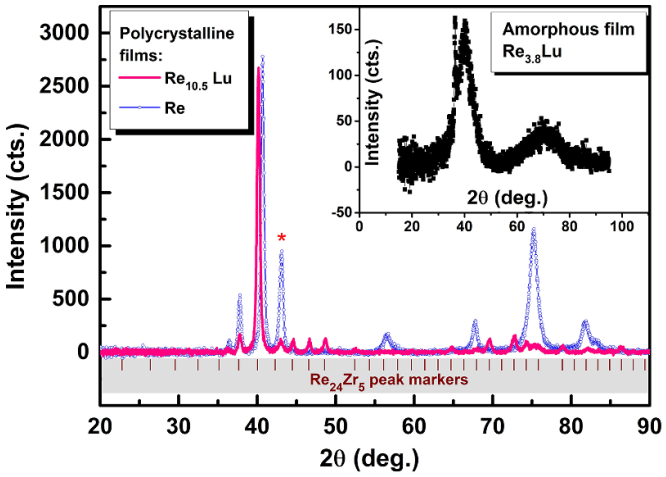

Figure 3. Grazing incidence x-ray diffraction pattern of polycrystalline $Re_{10.5}Lu$ film compared to that of pure Re film [30]. Inset corresponds to amorphous film $Re_{3.8}Lu$. Asterisk indicates a peak which does not belong to the $Re_{24}Zr_5$ dataset (the latter is shown in the shaded grey zone). It coincides with pure Re peak.

Table 2. Crystal lattice parameters comparison.

	a, Å	b, Å	c, Å	volume, Å^3	space group
Re, bulk [24–26]	2.761	2.761	4.458	29.430	$P63/mmc$
Re, film [30]	2.782	2.782	4.484	30.053	$P63/mmc$
$Re_{10.5}Lu/Re_{24}Zr_5$	9.5743(5)	9.5743(5)	9.5743(5)	877.636	$217 : I\bar{4}3m$

on an actual powder specimen, which will be left for future studies. Table 2 shows the crystal structure parameters of Re and $Re_{10.5}Lu/Re_{24}Zr_5$.

The results of magnetic and magnetotransport characterization of these films are shown in figures 4 and 5. Magnetic measurements of thin film properties are complicated by the presence of the substrate which is much more massive than the film itself. In our case, another complication is related with the smallness of H_{c1} which constitutes units of Oe. To address this complication, we applied demagnetization procedures before the measurements since the superconducting magnets of PPMS may have residual field of tens of Oe. In addition, the residual field shift after such procedures was determined for correcting the magnetic field values to actual zero, for example, by measuring the properties of calibration samples. As a result, the diamagnetic curve in figure 4, inset (a) has the required property $M(H = 0) = 0$. Moreover, the characteristic 'butterfly' patterns of polycrystalline film $Re_{10.5}Lu$ in figure 4, as well as for the amorphous film (inset (b) in figure 4) have the same required feature. Also, they both have a noticeable clockwise tilt caused by the substrate diamagnetism. Inset (b) demonstrates the 'butterfly' of $Re_{3.8}Lu$

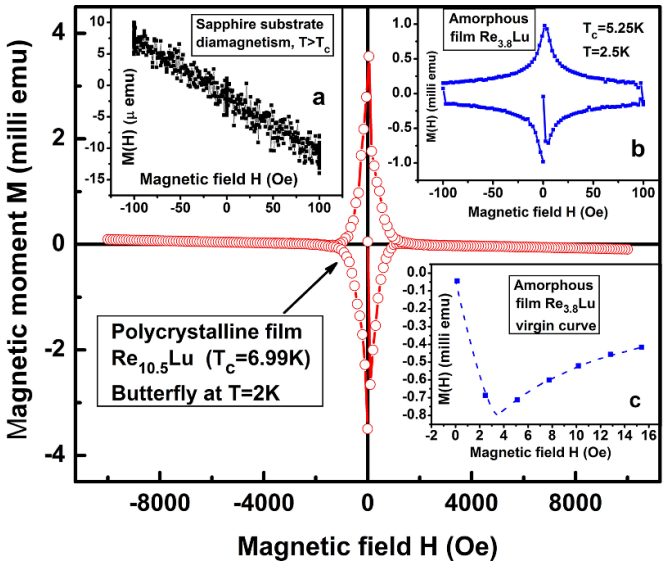

Figure 4. Magnetic moment vs. magnetic field of polycrystalline film $Re_{10.5}Lu$ (main curve); of sapphire substrate (inset (a)); of amorphous film $Re_{3.8}Lu$ (inset (b)) with its virgin curve detailed in inset (c).

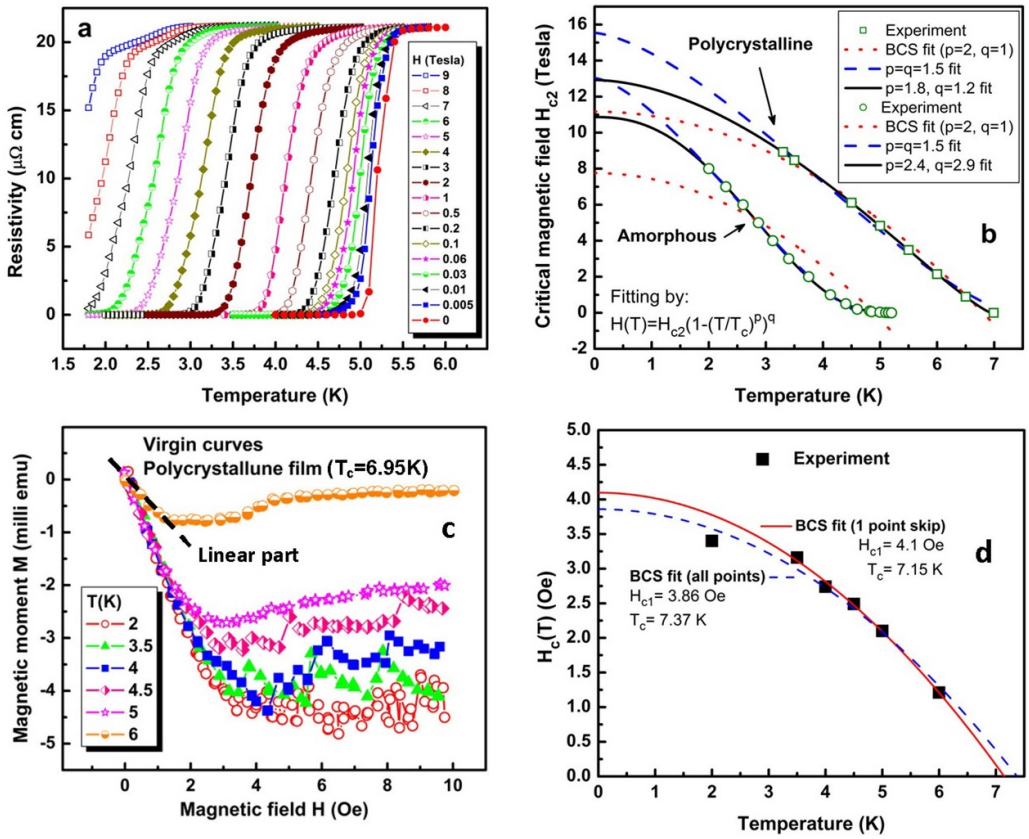

Figure 5. (a) Magnetotransport measurements for determining critical field H_{c2} vs. temperature in case of $x = 3.8$ (amorphous) film. Similar measurements were performed in case of $x = 10.5$ (polycrystalline) film. (b) Determining $H_{c2}(T = 0)$ for polycrystalline and amorphous films. The T_c value for each in-field measurement was chosen using the 50% criterion of the transition height of the resistivity curves. (c) Virgin curves of polycrystalline film at various temperatures for determining the value of H_{c1} (panel d). This value of H_{c1} is constructed in (d) using the linear part of experimental data (one such line is shown in panel c—dashed line for $T = 6$ K data) via modeling in accordance with the relation $H_{c1}(T) = H_{c1}(0)[1 - (T/T_c)^2]$.

Table 3. Summary of parameters of the representative superconductors.

	H_{c1}, Oe	H_{c2}, T	$\xi(0)$, nm	$\lambda_L(0)$, nm	κ
Amorphous ($x \approx 3.8$)	3.88	11	5.5	4.87	0.89
Polycrystalline ($x \approx 10.5$)	4	13	5.05	4.48	0.89

amorphous film. Its zoomed-in virgin curve (inset (c)), in addition to demonstrating the Meissner effect, confirms the required accuracy in our magnetic measurements. As follows from this figure 4(c) and the calculations of Ginzburg–Landau parameter κ below, one should expect trapped flux in the measurement results presented in figure 1(b).

4. Discussion

As follows from table 1, both stoichiometric ratio and substrate's temperature affect the crystalline properties of this material. Moreover, the stoichiometric ratio itself depends on the substrate temperature at deposition. The last entry in table 1 corresponds to less than 1%(at.) of Lu in the composition—we reached here the resolution limit of our EDS. Meanwhile, as follows from [30], pure Re films grown in similar conditions (600 °C) are amorphous and do not superconduct down to 1.8 K, and when grown at 30 °C they superconduct at 3.6 K. The role of the substrate-film interplay is also important; for example, bulk Re does not superconduct above 1.8 K [24].

Our samples' H_{c2} (T) curves show different behavior compared to the conventional BCS dependence $H_{c2}(T) = H_{c2}(0)[1-(T/T_c)^2]$. Therefore, following [34, 35] the curves can instead be fitted using the expression $H_{c2}(T) = H_{c2}(0)[1-(T/T_c)^p]^q$ where the exponents $p = q$ were chosen to be 3/2. A slightly better fit to the data can be obtained when the constraints on p and q are removed by choosing $p = 1.8$, $q = 1.2$. This fit is shown in figure 5(b) which yields $H_{c2} \approx 13$ T. Using the Ginzburg–Landau relation $H_{c2} = \phi_0/(2\pi\xi^2)$, where $\phi_0 = 2.068 \times 10^{-15}$ Wb is the flux quantum [36], the estimated coherence length of our film with $T_c = 6.95$ K is $\xi(0) = 5.05$ nm.

Combining $\xi(0)$ and the estimate for H_{c1} from panel (d) in figure 5 ($H_{c1} \sim 4$ Oe)[2] into the standard expression $H_{c1} = [\phi_0/(4\pi\lambda_L^2)][ln(\lambda_L/\xi) + 0.12]$ [37], the estimate for our film's magnetic penetration depth is $\lambda_L(0) \approx 4.48$ nm. Finally, the Ginzburg–Landau parameter can also be calculated, $\kappa = \lambda_L/\xi = 0.89$, which shows that our film, being of type-II, is rather close to the theoretical boundary separating type-I and type-II superconductors of $\kappa = 1/\sqrt{2} \approx 0.71$. This value of κ for polycrystalline $Re_{10.5}Lu$ matches with the reported values for pure Re films [30], though the individual values of λ_L and ξ are different.

For the amorphous $Re_{3.8}Lu$ with $T_c \approx 5.3$ K, the value of H_{c2} is a bit smaller: $H_{c2} \approx 11$ T (second curve in figure 5(b), obtained with the fitting parameters $p = 2.4$ and $q = 2.9$) yielding an estimate: $\xi = 5.5$ nm. From figure 4(c), $H_{c1}(T = 2.5\text{ K}) \approx 3$ Oe. Taking into account that $H_{c1}(T = 5.3\text{K}) = 0$, one can use parabolic approximation as above and obtain an estimate $H_{c1}(0) \approx 3.88$ Oe[3]. This yields $\lambda_L(0) \approx 4.87$ nm and $\kappa = 0.89$, as in the case of polycrystalline films. Table 3 contains extracted values of these data.

5. Summary

We introduced a new material, Re_xLu ($3.8 \leqslant x \leqslant 99+$). In particular, $Re_{10.5}Lu$ exceeds the critical temperature of known Re_6Hf, Re_6Zr and Re_6 Ti. While these predecessors have never been reported having $T_c > 6$ K, either in bulk or thin film form, $Re_{10.5}Lu$ demonstrated $T_c \approx 7$ K. Thus, the idea that Lu can successfully play the role of a transition element in Re–Lu compound is confirmed by this research. By analogy, one can expect that this NCS material will also break TRS. It will be very interesting to explore that property, though that goal is beyond this paper. The indirect proof of broken TRS may be obtained by effects related to nonreciprocal current control devices made of this material: demonstration of nonreciprocity in absence of applied magnetic field may serve as such a proof.

The simplicity of the described deposition method may facilitate the application of this material for the range of devices mentioned in Introduction. Also, the information obtained by our research may provide grounds for further fundamental studies based on band-structure computations of superconducting state in Re–Lu materials to quantitatively explain the discovered features including fitting parameters p and q for H_{c2} curves. Finally, the parameters λ_L and ξ estimated above may be used for modeling of phenomena in Re–Lu-based superconducting devices.

[2] In this fitting procedure, the value of T_c is a free parameter. As follows from figure 5(d), its value is close to the experimental $T_c \approx 7$ K.

[3] In this fitting procedure, the experimental value of T_c is used, and the parabola is enforced to go through 2 points: $H_{c1}(T_c) = 0$ and $H_{c1}(2.5\text{ K}) \approx 3$ Oe. This method is less accurate, however, it is satisfactory for estimates.

Data availability statement

All data that support the findings of this study are included within the article (and any supplementary files).

Acknowledgments

This research was supported by the ONR Grant Nos. N00014-21-1-2879, N00014-20-1-2442 and N00014-23-1-2866. We are grateful to Physics Art Frontiers for technical assistance.

Appendix A. Compositional analysis

Compositional analysis was performed using standard energy-dispersive x-ray spectroscopy in scanning electron microscope, as was mentioned in the main text. The results were accumulated and averaged from many points. They were also acquired via mapping. These two methods revealed consistently similar values, which yield a Re to Lu ratio of about 10.5, as indicated in figure A1.

Similar analysis was performed for the amorphous film which revealed the ratio ∼3.8. The plotted EDS spectrum contains the peaks of the film as well as those belonging to the sapphire (Al_2O_3) substrates (carbon is always present during EDS analysis). To minimize the substrate interference, we performed measurements below maximum energy (= 30 keV). At 20 keV the spread of compositional data between the measured points becomes acceptably small.

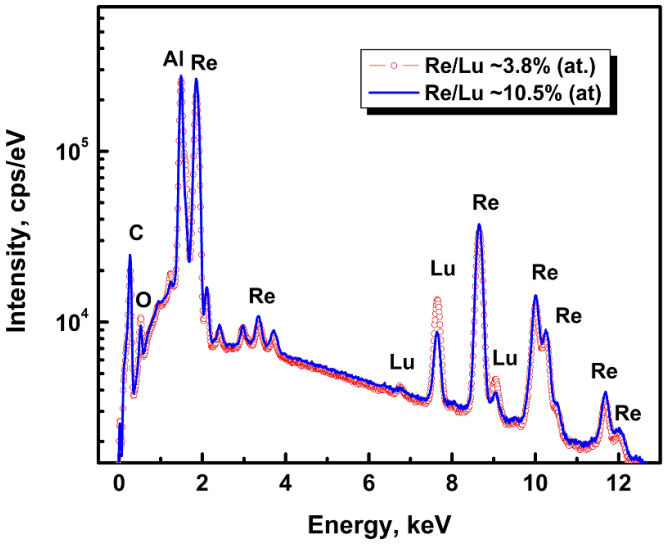

Figure A1. EDS data from polycrystalline and amorphous samples.

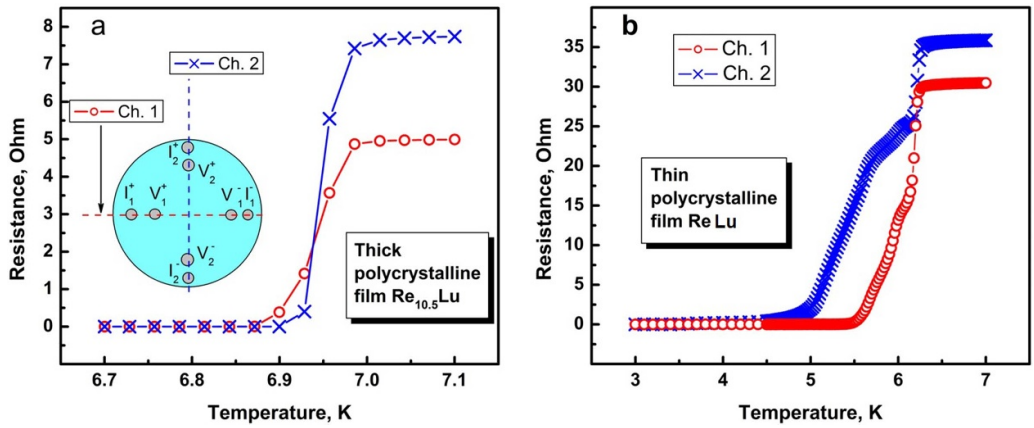

Figure B1. Testing lateral homogeneity of (a) thick and (b) thin polycrystalline films.

Appendix B. Multichannel resistivity measurements

To characterize the phase homogeneity of deposited films we used resistivity measurements described in figure B1. In this figure, the large circle indicates thin film (8 mm in diameter) with 2 sets of 4-probe contacts (schematically notated as $I_{1,2}^{+/-}$ and $V_{1,2}^{+/-}$) placed in mutually orthogonal directions for channels 1 and 2. At each temperature step, PPMS consecutively performed measurements for these channels. The plotted data are indicative of very good compositional homogeneity in relatively thick films (thickness $d \geqslant 100$ nm). Thinner films ($d \sim 30$ nm) are less perfect though still can be utilized in devices biased at helium temperatures.

Appendix C. X-ray reflectivity measurements

X-ray reflectivity (XRR), as was first noticed by Kiessig in 1931 [38] (more recent references and the detailed description of this method can be found in [39]) can be used for characterization of thin film quality, as explained in figure C1.

In particular, it allows us to model the density, thickness, and roughness of the deposited film and its surface layer. We used the Simple Reflectivity Model of free software GenX [40] for processing our Rigaku SmartLab data, figure C1. It yields the parameters: film thickness = 311 Å, density = 17.5 g cm^{-3}, roughness = 3 Å; top surface layer thickness = 10 Å, density = 16.1 g cm^{-3}; and substrate roughness 4 Å. For comparison, we presented in figure C1 also a similar curve obtained for Re–Nb film, which was recently used for achieving high-quality Dayem bridges [41]. The comparison demonstrates obvious superiority of Re–Lu film in surface and possibly interface roughness which is important for nanoscale devices.

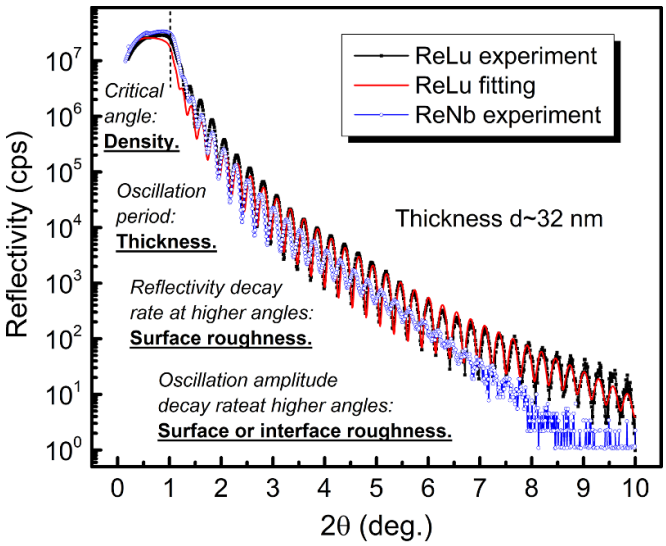

Figure C1. XRR curves for Re–Lu and Re–Nb films. The modeled curve for ReLu film which yields the parameters mentioned in the text is also shown.

ORCID iDs

Serafim Teknowijoyo https://orcid.org/0000-0002-5542-5482
Armen Gulian https://orcid.org/0000-0002-4695-4059

References

[1] Tokura Y and Nagaosa N 2018 *Nat. Commun.* **9** 3740
[2] Wakatsuki R and Nagaosa N 2018 *Phys. Rev. Lett.* **121** 026601
[3] Hoshino S, Wakatsuki R, Hamamoto K and Nagaosa N 2018 *Phys. Rev.* B **98** 054510

[4] Ando F, Miyasaka Y, Li T, Ishizuka J, Arakawa T, Shiota Y, Moriyama T, Yanase Y and Ono T 2020 *Nature* **584** 373–6
[5] Ideue T and Iwasa Y 2020 *Nature* **584** 349–50
[6] Lyu Y Y *et al* 2021 *Nat. Commun.* **12** 2703
[7] Baumgartner C *et al* 2022 *Nat. Nanotechnol.* **17** 39–44
[8] Wu H, Wang Y, Xu Y, Sivakumar P K, Pasco C, Filippozzi U, Parkin S S P, Zeng Y J, McQueen T and Ali M N 2022 *Nature* **604** 653–6
[9] Strambini E *et al* 2022 *Nat. Commun.* **13** 2431
[10] Morimoto T and Nagaosa N 2018 *Sci. Rep.* **8** 2973
[11] Chahid S, Teknowijoyo S, Mowgood I and Gulian A 2023 *Phys. Rev.* B **107** 054506
[12] Teknowijoyo S, Chahid S and Gulian A 2023 *Phys. Rev. Appl.* **20** 014055
[13] Anwar M S, Nakamura T, Ishiguro R, Arif S, Robinson J W A, Yonezawa S, Sigrist M and Maeno Y 2023 *Commun. Phys.* **6** 290
[14] Shang T *et al* 2018 *Phys. Rev. Lett.* **121** 257002
[15] Singh D, Sajilesh K P, Barker J A T, Paul D M, Hillier A D and Singh R P 2018 *Phys. Rev.* B **97** 100505
[16] Shang T *et al* 2018 *Phys. Rev.* B **97** 020502
[17] Singh D, Barker J A T, Thamizhavel A, Paul D M, Hillier A D and Singh R P 2017 *Phys. Rev.* B **96** 180501
[18] Singh R P, Hillier A D, Mazidian B, Quintanilla J, Annett J F, Paul D M, Balakrishnan G and Lees M R 2014 *Phys. Rev. Lett.* **112** 107002
[19] Samkharadze N, Bruno A, Scarlino P, Zheng G, DiVincenzo D P, DiCarlo L and Vandersypen L M K 2016 *Phys. Rev. Appl.* **5** 044004
[20] Borisov K *et al* 2020 *Appl. Phys. Lett.* **117** 120502
[21] Hazard T M, Gyenis A, Di Paolo A, Asfaw A T, Lyon S A, Blais A and Houck A A 2019 *Phys. Rev. Lett.* **122** 010504
[22] Grünhaupt L *et al* 2019 *Nat. Mater.* **18** 816–9
[23] Niepce D, Burnett J and Bylander J 2019 *Phys. Rev. Appl.* **11** 044014
[24] Alekseevskii N E, Mikheeva M N and Tulina N A 1967 *Sov. Phys.-JETP* **25** 575
Alekseevskii N E, Mikheeva M N and Tulina N A 1967 *Z. Eksp. Teor. Fiz.* **52** 875
[25] Roberts B W 1976 *J. Phys. Chem. Ref. Data* **5** 581–822
[26] Song C, Heitmann T W, DeFeo M P, Yu K, McDermott R, Neeley M, Martinis J M and Plourde B L T 2009 *Phys. Rev.* B **79** 174512
[27] Haq A and Meyer O 1982 *Thin Solid Films* **94** 119–32
[28] Frieberthauser P E and Notarys H A 1970 *J. Vac. Sci. Technol.* **7** 485–8
[29] Pappas D P *et al* 2018 *Appl. Phys. Lett.* **112** 182601
[30] Teknowijoyo S and Gulian A 2023 *Opt. Mem. Neur. Netw.* **32** S327–33
[31] Volovik G E and Gor'kov L P 1985 *Zh. Exp. i Teor. Fiz.* **88** 1412 (available at: www.jetp.ras.ru/cgi-bin/e/index/e/61/4/p843?a=list)
[32] Scerri E 2012 *Chem. Int.* **34** 28–31
[33] Jensen W B 1982 *J. Chem. Educ.* **59** 634
[34] Biswas P K, Lees M R, Hillier A D, Smith R I, Marshall W G and Paul D M 2011 *Phys. Rev.* B **84** 184529
[35] Micnas R, Ranninger J and Robaszkiewicz S 1990 *Rev. Mod. Phys.* **62** 113–71
[36] Brandt E H 1988 *Phys. Rev.* B **37** 2349–52
[37] Tinkham M 1975 Introduction to Superconductivity *International Series in Pure and Applied Physics* (McGraw-Hill)
[38] Kiessig H 1931 *Ann. Phys., Lpz.* **402** 715–68
[39] Vignaud G and Gibaud A 2019 *J. Appl. Crystallogr.* **52** 201–13
[40] Glavic A and Björck M 2022 *J. Appl. Crystallogr.* **55** 1063–71
[41] Koch J *et al* Gate-controlled supercurrent effect in dry-etched Dayem bridges of non-centrosymmetric niobium rhenium *Nano Lett.* submitted